Numerical modelling of acoustic scattering by smooth inclusions in a layered fluid-solid medium

Ilkka Karasalo

National Defence Research Institute
Hydroac. Environment and Active Sonar
S - 172 90 Stockholm, Sweden
Email: ilkka@sto.foa.se

Johan Mattsson

Royal Institute of Technology
The Marcus Wallenberg Laboratory
S - 100 44 Stockholm, Sweden
Email: johanm@fkt.kth.se

Abstract

A boundary integral equation (BIE) method is described for computing the scattering of a monofrequent acoustic field by a smooth, rigid 3D object in a layered range-independent fluid-solid medium.

The BIE is discretized using B-splines (BSP), point collocation and high-order numerical integration. The discretized equations are solved by an iterative method, enhanced by pre-conditioning with the LU factors of a related linear system for spline interpolation on the scatterer surface.

Numerical examples are given at frequencies of a few kHz, representative e.g. for a parametric transducer. The BSP method is shown to provide order-of-magnitude gains in computation times compared to a standard BEM technique with quadratic elements as frequency increases and/or accuracy requirements are tightened.

1. Introduction

Acoustic scattering from a 3D obstacle inside a range-independent layered fluid-solid medium is an important model problem with numerous applications in underwater acoustics. The fundamental problem - to predict the scattered wavefield for a given source-medium-scatterer-receiver configuration is of interest both in its own right, and, in practice perhaps more frequently, in the inverse problem of detecting and classifying scattering objects by analysis of returned echoes, [1] and references therein. In all but the simplest model cases - notably with a spherical or cylindrical scatterer and a medium composed of very few homogeneous layers - a closed-form analytical solution of the scattered field is not available. The design of methods for numerical modelling of scattering has therefore received much effort in the past few decades and has, together with the rapid development of technology for large-scale numerical computation, brought increasingly complex scattering scenarios within computational reach.

Boundary integral equation (BIE) methods for the modelling of scattering are particularly useful whenever the Green's function of the surrounding medium may be computed efficiently. Among their advantages are (i) the spatial dimension and thus the number of unknowns in the discretized equations is reduced, (ii) the boundary, the interface and the far-field radiation conditions in the surrounding medium are satisfied *a priori*. Examples of BIE modelling of the scattering of underwater sound are [2] where the surface of an acoustically penetrable scatterer is discretized by linear boundary elements, and [3] treating a cylindrically structured scatterer at the interface between two homogeneous fluid halfspaces.

Except for low-frequency fields in simple media and simple scatterer geometries, the BIE approach is computationally demanding, with workload and memory requirements increasing rapidly with frequency: If point collocation with a p'th order method is used for discretisizng the BIE, a crude estimate of the required number of meshpoints on the scatterer surface is $N \approx (ka\ (C/\epsilon)^{1/p})^2$ where k is is the wavenumber, a an average diameter of the scatterer, ϵ is the wanted relative accuracy and C is the error constant of the method of discretization. For example, for the trapezoidal rule $C = 1/12, p = 2$ giving $N \approx 320$ for $ka = 2, \epsilon = 0.001$. For many methods, e.g. FEM with Lagrange-type elements, the discretized BIE has the form of a dense linear system of equations with dimension equal to or close to N. The main computational tasks in a BIE approach are the assembly and solution of this system, and the subsequent computation of the scattered field at say M wanted points in the medium using the surface integral representation. The computational work for these tasks are proportional to at least N^2 (N^3 if a direct method is used) and MN, respectively. It is therefore interesting to note that increasing the order in the above estimate to $p = 4$ reduces the required number of meshpoints to $N = 36$.

In this paper we describe a recently developed BIE method for modelling scattering by smooth 3D bodies immersed in a range-independent fluid-solid medium. The Green's function of the medium is computed by an adaptive, accurate transform integral method [4]. The BIE is discretized by point collocation using high-order B-spline (BSP) basis functions. The collocation integrand is formulated in 'tilted' spherical coordinates θ', ϕ' making it smooth in both variables and periodic in ϕ', and the collocation integrals are computed by high-order schemes.

Sections 2 - 3 review the basic equations of the BIE approach and present the B-spline collocation method. In section 4 numerical examples are presented for super-ellipsoidally shaped rigid scatterers at a few kHz, representative for a parametric bottom-penetrating transducer. A conventional BEM method with second-order elements [5] is used for numerical comparisons. The BSP technique is demonstrated to be highly efficient, providing order-of-magnitude gains in computation time as the frequency increases and/or the accuracy requirements are tightened.

2. The BIE formulation

Consider an acoustically rigid, smooth 3D object submerged in a fluid layer in a range-independent layered fluid-solid medium, cf. fig. 1. A cartesian coordinate system is introduced as shown, with a vertical, downward pointing z axis and origin at water surface. The medium parameters are assumed to be continuous functions of z within each layer, with jump discontinuities allowed at layer boundaries. The materials are modelled as isotropic, with viscous attenuation represented by complex wavespeeds. The wavefield is excited by a vertical array of time harmonic point sources on the z-axis within the water column.

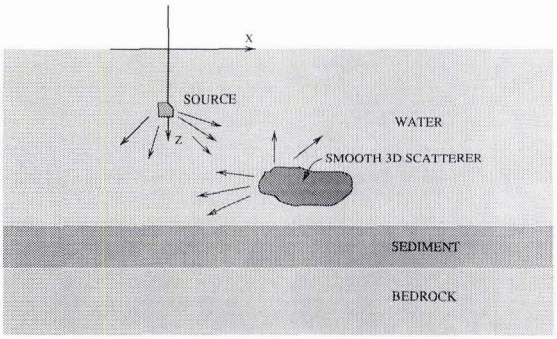

Figure 1: Geometry of model problem.

By the scalar Green's theorem, the 'density scaled' complex pressure $q(\mathbf{r}) = \rho^{-1}(\mathbf{r})p(\mathbf{r})$ at a point $\mathbf{r}_0$ inside a fluid layer is given by

$$q(\mathbf{r}_0) = q^{(in)}(\mathbf{r}_0) - \int_S \nabla_1 g(\mathbf{r}, \mathbf{r}_0) \cdot \hat{\mathbf{n}}(\mathbf{r}) q(\mathbf{r}) dS(\mathbf{r}). \tag{1}$$

S is the surface of the scatterer, $g(\mathbf{r}, \mathbf{r}_0)$ the Green's function of the layered medium, and $q^{(in)} = \rho^{-1}(\mathbf{r})p^{(in)}$ where

$p^{(in)}$ is the incident field, i.e. the field excited by the source in a scatterer-free medium. An integral equation of the second kind for $q(\mathbf{r})$, $\mathbf{r} \in S$, is obtained from (1) in the limit as $\mathbf{r}_0 \to S$,

$$\frac{1}{2}q(\mathbf{r}_s) + \int_S \nabla_1 g(\mathbf{r}, \mathbf{r}_s) \cdot \bar{\mathbf{n}}(\mathbf{r}) q(\mathbf{r}) dS(\mathbf{r}) = q^{(in)}(\mathbf{r}_s). \tag{2}$$

See for example Ström [6, Ch. 2, Sec. 5.4] for a derivation in the free space case. For a smooth surface S, the kernel of the integral in (2) is an equally smooth function of $\mathbf{r}$, except for an integrable $|\mathbf{r} - \mathbf{r}_s|^{-1}$ singularity at $\mathbf{r}_s$. If $g(\mathbf{r}, \mathbf{r}_0)$ and $p^{(in)}$ are (numerically) known, then (2) can be solved numerically, and the pressure field in the medium subsequently computed from (1).

3. A high-order B-spline collocation method

3.1. The B-spline basis

We assume the surface of the scatterer to be defined by a many times differentiable ('smooth') function

$$\mathbf{r} = \mathbf{r}_S(\theta, \phi) \qquad 0 \le \theta \le \pi \qquad 0 \le \phi \le 2\pi \tag{3}$$

where (θ, ϕ) are the spherical angle coordinates of a cartesian coordinate system with origin fixed inside the scatterer. A rectangular, equidistant grid of knotpoints (θ_j, ϕ_i)

$$\theta_j = (j-1)k \quad , \quad \phi_i = (i-1)h \quad , \quad k = \frac{\pi}{M-1} \quad , \quad h = \frac{2\pi}{N}. \tag{4}$$

is introduced, together with associated bases of B-splines [7, Ch. 19] $G_j(\theta)$ and $F_i(\phi)$ with degrees k_G and k_F, and support in $\theta_j \le \theta \le \theta_{j+k_G+1}$ and $\phi_i \le \phi \le \phi_{i+k_F+1}$, respectively. We seek an approximation $\hat{q}(\theta, \phi)$ to the solution of (2) of the form

$$\hat{q}(\theta, \phi) = \sum_{i=1-k_F}^{N} \sum_{j=1-k_G}^{M-1} \gamma_{ij} G_j(\theta) F_i(\phi). \tag{5}$$

At any (θ, ϕ) the number of nonzero terms in this expansion is at most $(k_F + 1)(k_G + 1)$. Thus the work for computing $\hat{q}(\theta, \phi)$ for given (θ, ϕ) and $\{\gamma_{ij}\}$ does not grow with the total number of terms $(N + k_F)(M - 1 + k_G)$ in the expansion.

To ensure that $\hat{q}(\theta, \phi)$ has spline-like continuity everywhere on the unit sphere, the coefficients γ_{ij} are required to satsify the following *a priori* conditions. First,

$$\gamma_{ij} = \gamma_{(i+N+1)j} \quad , \quad i = 1 - k_F, \ldots, 0 \quad , \quad j = 1 - k_G, \ldots, M - 1, \tag{6}$$

to ensure the periodicity in ϕ. Second, the number N of ϕ knot steps is restricted to be even, and

$$\hat{q}(0, \phi_j) = \hat{q}(0, \phi_1) \qquad \hat{q}(\pi, \phi_j) = \hat{q}(\pi, \phi_1) \qquad j = 2, \ldots, N, \tag{7}$$

$$\frac{\partial^l \hat{q}(0, \phi_i)}{\partial \theta^l} = (-1)^l \frac{\partial^l \hat{q}(0, \phi_{i+N})}{\partial \theta^l} \quad , \quad \frac{\partial^l \hat{q}(\pi, \phi_i)}{\partial \theta^l} = (-1)^l \frac{\partial^l \hat{q}(\pi, \phi_{i+N})}{\partial \theta^l} \qquad \begin{matrix} i = 1, \ldots, N/2 \\ l = 1, \ldots, k_G - 1. \end{matrix} \tag{8}$$

Equations (7) and (8) ensure that the smoothness of $\hat{q}$ as function of θ at the 'poles' $\theta = 0$ and $\theta = \pi$ is the same as at other knotpoints. From symmetry properties of the B-spline basis functions follows that (6) - (8) are linearly independent for odd degrees only, and thus k_F and k_G are restricted to be odd for simplicity.

3.2. Computation of the collocation integrals

Equations (6) - (8) impose $k_F(M-1+k_G)$, $2(N-1)$ and $(k_G-1)N$ linear constraints, respectively, on the $(N+k_F)(M-1+k_G)$ coefficients of (5). The remaining $N(M-2)+2$ degrees of freedom are fixed by requiring $\tilde{q}(\theta,\phi)$ to satisfy the BIE, (2), at $(0,\phi_1)$, (π,ϕ_1) (the poles) and at the $N(M-2)$ non-polar knotpoints.

A high-order numerical scheme for the collocation integrals must be chosen with proper care for the (mild) singularity of the kernel of (2) at the collocation point $\mathbf{r}_s$. The following behaviour of the kernel near $\mathbf{r}_s$ is easily verified in a homogeneous space, and is conjectured to hold also for layered media.

For a given $\mathbf{r}_s$, let the surface S be defined by a smooth function $\mathbf{r}(\xi,\eta)$ such that $\mathbf{r}_s=\mathbf{r}(0,0)$ and the tangent vectors $\mathbf{r}_\xi(0,0)$ and $\mathbf{r}_\eta(0,0)$ are linearly independent. Let γ,χ be polar coordinates in the (ξ,η) plane, i.e.

$$\xi=\xi(\gamma,\chi)=\gamma\cos(\chi) \qquad \eta=\eta(\gamma,\chi)=\gamma\sin(\chi) \tag{9}$$

Then, as function of (γ,χ) the integrand in (2) has the form

$$\nabla_1 g(\mathbf{r},\mathbf{r}_s)\cdot\hat{\mathbf{n}}(\mathbf{r})\tilde{q}(\mathbf{r})dS(\mathbf{r}) \quad = \quad k(\gamma,\chi)\tilde{q}(\mathbf{r}(\gamma,\chi))d\gamma d\chi \tag{10}$$

where for some $\gamma_0>0$ the kernel $k(\gamma,\chi)$ is smooth in the closed rectangle $0\le\gamma\le\gamma_0 \quad 0\le\chi\le 2\pi$. Its limit value $k(0,\chi)$ at the collocation point is a smooth function of χ with period π.

Thus, the kernel as function of 'polar-like' coordinates on S with origin at $\mathbf{r}_s$ remains smooth and bounded when $\mathbf{r}_s$ is approached along S from any given direction. Since by (6) - (8) $\tilde{q}(\mathbf{r})$ is smooth everywhere on S, this behaviour holds also for the collocation integrand.

Then, by introducing tilted spherical angle coordinates (θ',ϕ') with the north pole $\theta'=0$ at the collocation point $\mathbf{r}_s=\mathbf{r}_S(\theta_i,\phi_j)$ (cf. (3)) the BIE takes the form

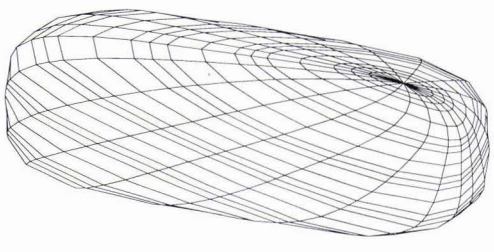

Figure 2: Gridpoints for a collocation integral by use of tilted coordinates (θ',ϕ')

$$\frac{1}{2}\tilde{q}(0,0)+\int_0^{2\pi}\int_0^{\pi} k(\theta',\phi',0,0)\;\tilde{q}(\theta',\phi')\;d\phi'\;d\theta' = q^{(in)}(0,0) \tag{11}$$

cf. fig. 2. The integrand is a smooth function in the closed region of integration, periodic in ϕ' with period 2π. A high-order numerical scheme for this integral is obtained e.g. by combining the trapezoidal rule in ϕ' (the periodicity ensuring super-polynomial order of convergence see e.g. [8, Sec 7.4.4]), and a scheme with the wanted order in θ'. The numerical results presented below were obtained with θ'-schemes of even order, based on linear combination of trapezoidal sums at multiple stepsizes and polynomial extrapolation [9, Sec. 3.3]

By eliminating γ_{ij} with negative i using (6), inserting (5) into (11) and applying the numerical integration scheme, the BIE together with (7) and (8) take the form of a linear system of equations

$$\begin{bmatrix}\mathbf{A}_r\\ \mathbf{A}_c\end{bmatrix}\mathbf{x} \;=\; \begin{bmatrix}\mathbf{0}\\ \mathbf{b}_i\end{bmatrix} \tag{12}$$

$\mathbf{A}_r$ corresponds to (7)-(8) and is $\{N(k_G+1)-2)\}\times\{N(M-1+k_G)\}$ and sparse. $\mathbf{A}_c$ is a dense $\{N(M-2)+2\}\times\{N(M-1+k_G)\}$ matrix of the coefficients of the discretized BIE, and $\mathbf{b}_i$ contains the values of the incident field at the collocation points. The components of $\mathbf{x}$ are the $N(M-1+k_G)$ unknown coefficients γ_{ij} with $i\ge 0$ in (5).

3.3. Solution of the discretized integral equation

Omitting the contribution from the collocation integrals at the assembly of (12) gives a linear system

$$\begin{bmatrix} \mathbf{A}_r \\ \mathbf{A}_i \end{bmatrix} \mathbf{x}^{(in)} = \begin{bmatrix} \mathbf{0} \\ \mathbf{b}_i \end{bmatrix} \tag{13}$$

$\mathbf{A}_i$ represents the term $\frac{1}{2}\hat{q}(0,0)$ of (11), and the components of $\frac{1}{2}\mathbf{x}^{(in)}$ are coefficients $\gamma_{ij}^{(in)}$ of a B-spline expansion interpolating to the incident field at the collocation points.

The coefficient matrix of system (13) is real-valued and sparse, containing at most $(k_F+1)(k_G+1)$ nonzero elements per row. It can be stored compactly and LU-decomposed using sparsity conserving pivoting [10], at a computational cost which is insignificant compared to that of solving (12).

An economical method for solving (12), is then to use an iterative method for nonsymmetric linear systems like the generalized minimum residual method [11], enhanced by preconditioning with the LU factors of system (13). In the numerical examples below, this technique was found to reduce the execution time for solving (12) by a factor of ten or more compared to direct LU decomposition already for systems of moderate size.

4. Numerical examples

In this section we present some numerical examples using a scatterer with superellipsoidal shape, cf. (3),

$$\mathbf{r}_S(\theta,\phi) = \|\hat{\mathbf{r}}\|_p^{-1}\mathbf{D}\hat{\mathbf{r}} \tag{14}$$

where $\hat{\mathbf{r}} = \hat{\mathbf{r}}(\theta,\phi) = (\sin(\theta)\cos(\phi), \sin(\theta)\sin(\phi), \cos(\theta))$, $\|(x,y,z)\|_p = (|x|^p + |y|^p + |z|^p)^{1/p}$ with $p \geq 2$, and $\mathbf{D}$ a diagonal 3×3 matrix with the half-axis lengths a, b, c as diagonal elements.

The incident field is generated by a monofrequent vertical point-source array with length 15 m and center at depth 10 m. The array is steered and weighted to emit a downward-pointing endfire beam with small sidelobes, modelling the beam from a parametric transducer, fig. 3. An adaptive transform-integral method [4] is used to

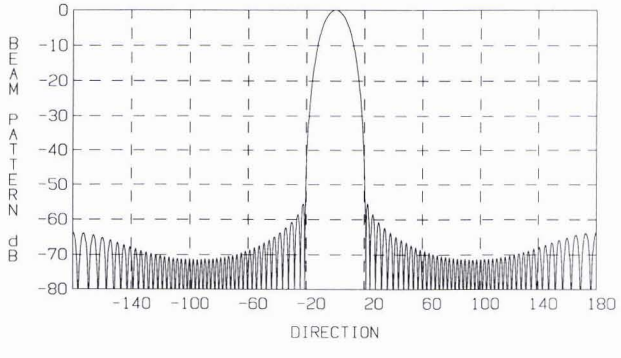

Figure 3: Beam pattern of the source array at 2000 Hz.

compute tables of the incident field and the Green's function of the layered medium on 3D-grids of (source depth, receiver depth, horizontal source-receiver range) values covering the scatterer and the spatial region of interest. The Green's function values for assembling (12) and computing the total field from (1) are obtained by high-order 3D spline interpolation in such tables.

In all examples shown the degree of the B-spline base functions in (5) was $k_F = k_G = 5$. The order of the quadrature scheme for the latitude coordinate (θ' in (11), θ in (1)) was 6, and the trapezoidal rule with a constant stepsize was used for the longitude coordinate. The number of collocation points was adapted in each case to provide visual convergence in plots of the scattered field, i.e. $\approx 1\%$ relative error in complex pressure values. The number of quadrature points was twice the number of collocation points in both coordinates.

Our examples are of two types. First, in sec. 4.1 the performance of the B-spline method is compared to a standard algorithm at selected frequencies for a scatterer in a homogeneous water half-space. The reference algorithm is a boundary element method (BEM), with triangular elements and quadratic basis functions of Lagrange type [5]. Second, in sec. 4.2 the field from a scatterer buried inside a fluid sediment is computed at a dense grid in the upper water column. Greyscale plots are displayed of the interference pattern of the scattered field both for a sediment halfspace, and for a finite sediment layer bounded by a rock halfspace.

4.1. A benchmark case with simple geometry

In our first example the medium is a homogeneous halfspace of water with sound speed 1450 m/s and density 1000 kg/m^3. The scatterer is a rigid superellipsoid defined by (14) with exponent $p = 4$ and half axes $a = 0.5$ m, $b = 0.5$ m and $c = 1.0$ m. The c axis is vertical and the center of the scatterer is on the z-axis at depth $z_c = 40$ m. The scattered field was computed at 181 points along a half-circle with radius $R = 10$ m centered at the scatterer, $x_j = R\sin\theta_j, z_j = z_c + R\cos\theta_j, \theta_j = j\pi/180, j = 0, ..., 180$. The amplitude of the scattered field as function of scattering angle θ at frequency 1000 Hz is shown in fig. 4.

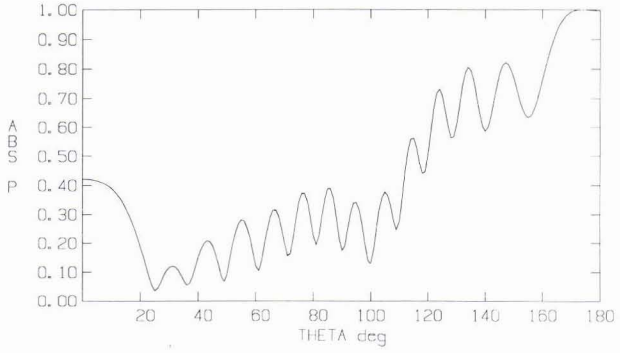

Figure 4: Amplitude of scattered field at range 10 m in the 1 kHz case in Table 1

Table 1 shows the number of unknowns in (12) and the execution times for assembly, solution and field computation at three source frequencies. Execution times refer to real time in (min:sec) on a dedicated HP C160 workstation.

Freq	Nr of unknowns		Assembly and solution		Field computation	
	BEM	BSP	BEM	BSP	BEM	BSP
500	642	192	0:55	0:05	0:04	0:04
750	1024	254	2:03	0:11	0:07	0:08
1000	2050	396	7:53	0:31	0:13	0:13

Table 1: Performance of the BSP and BEM methods

The efficiency of the B-spline method, in terms of execution time and storage space required for (12), is evident. A continuation of the benchmark to higher frequencies was not attempted due to the performance of the BEM algorithm.

The number of iterations required for solving (12) ranged from 7 to 20. No occurrence of a singularity of the kind discussed in [12] was observed in these examples or in the examples below.

4.2. Field from a buried scatterer

As final examples, we consider scattering by a rigid slender superellipsoid buried in a fluid sediment below 35 m of water. The shape of the scatterer is given by (14) with exponent $p = 4$ and half axes $a = 0.5$ m, $b = 0.5$ m

and $c = 2.5$ m. Again, the c axis is vertical and the center of the scatterer is on the z axis, 5 m below the seabed. The acoustic parameters of the sediment are $\rho = 1500\text{kg/m}^3$, $c_p = 1700\text{m/s}$ and attenuation $\beta_p = 0.2\text{dB}/\lambda$. The corresponding normalized half-axis lengths at 1000 Hz are $ka = 1.85$ and $kc = 9.25$.

Two types of seabed are considered, a sediment halfspace, and a 10 thick sediment layer bounded by a rock halfspace with elastic parameters $\rho = 2500$ kg/m^3, $c_p = 2500$ m/s, $c_s = 1800$ m/s, $\beta_p = 0.05\text{dB}/\lambda$ and $\beta_s = 0.2\text{dB}/\lambda$.

Figures 5-6 and 7-8 show greyscale plots of the amplitude of the scattered complex pressure in the region $r \leq 40$ m, $2 \leq z \leq 22$ m for the two media cases at frequencies 500 Hz and 1000 Hz, respectively. The field is normalized by the amplitude of the incident field at the scatterer depth in a water halfspace.

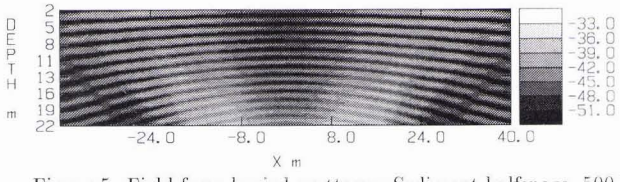

Figure 5: Field from buried scatterer: Sediment halfspace, 500 Hz

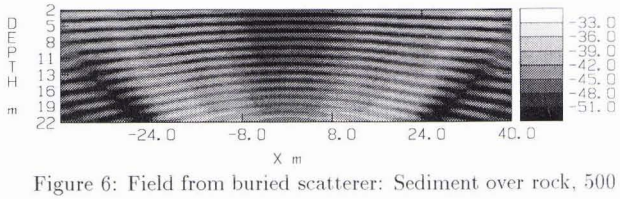

Figure 6: Field from buried scatterer: Sediment over rock, 500 Hz

In figures 5-6 it is interesting to note that the maximal amplitude of the scattered field occurs outside the z axis, thus favouring a bistatic source-receiver configuration. The influence of the bedrock on the strength of the backscattered field is small, however in the bedrock case the maximal amplitude is slightly shifted away from the z axis compared to the halfspace case.

At 1000 Hz, as shown in figures 6-7, the main lobe of the scattered field is on the z axis. The strength of the field is approximatively 10 dB higher than at 500 Hz. Finally, it is also seen here that the influence of the bedrock is very small, giving only a slight outward shift of the sidelobe pattern.

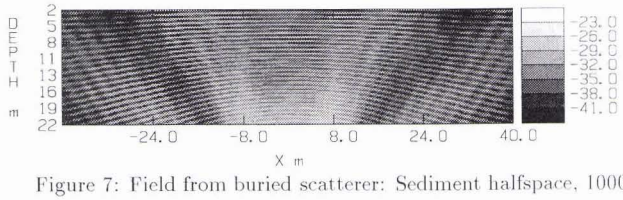

Figure 7: Field from buried scatterer: Sediment halfspace, 1000 Hz

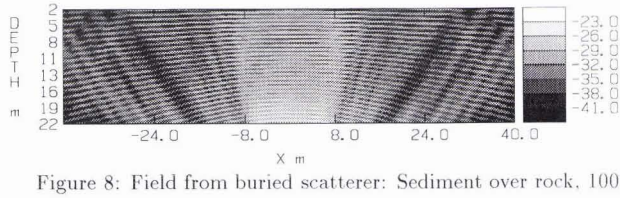

Figure 8: Field from buried scatterer: Sediment over rock, 1000 Hz

Acknowledgment

This work is part of the ISACS project, supported by the EU under contract MAS3-CT95-0046 (DG 12 - DTEE).

References

[1] G.C Gaunard and M.F. Werby, "Acoustic resonance scattering by submerged elastic shells", *Appl. Mech. Rev.*, vol 43, pp. 171-208, 1990.

[2] P. Gerstoft and H.Schmidt, "A boundary element approach to ocean seismoacoustic facet reverberation", *J. Acoust. Soc. Am.* **98**, pp. 1629-1642, 1991.

[3] J.A. Fawcett, "Acoustic scattering from cylindrical objects embedded between two half-spaces", *J. Acoust. Soc. Am.* **100**, pp. 3053-3060, 1996.

[4] I. Karasalo, "Exact finite elements for wave-propagation in range-independent fluid-solid media'. *J. Sound Vib.* **172**, pp. 671-688, 1994.

[5] K.E. Atkinson, "User's Guide to a Boundary Element Package for Solving Integral Equations on Piecewise Smooth Surfaces", Tech. Report 1994, Dept. of Mathematics, University of Iowa.

[6] V.V. Varadan, et.al., *Field representations and introduction to scattering*, Amsterdam, North-Holland, Ch 2, Sec. 5.4, pp. 73-90, 1991.

[7] M.J.D. Powell, *Approximation theory and methods*, Cambridge, Cambridge University Press, Ch 19, pp. 226-240, 1981.

[8] G. Dahlquist, Å. Björck, *Numerical methods*, Englewood Cliffs, Pretice-Hall, Sec. 7.4, pp. 297-301, 1974.

[9] J. Stoer, *Einführung in die Numerische Mathematik I*, Berlin, Springer, Sec. 3.3, pp. 108-117, 1972.

[10] A.R. Curtis and J.K. Reid, "The solution of large sparse unsymmetric systems of linear systems", AERE, Harwell, Report HL71/3280, June 1971.

[11] Y. Saad and M.H. Schultz, "A Generalized Minimal Residual Algorithm for Solving Nonsymmetric Linear Systems" *SIAM J. Sci. Stat. Comput.*, vol. 7, pp. 856-869, 1986.

[12] H.A. Schenk, "Improved integral formulation for acoustic radiation problems", *J. Acoust. Soc. Am.* **44**, pp. 41-58, 1968.